DE G

Fractional Calculus & Applied Analysis
An International Journal for Theory and Applications
VOLUME 24, NUMBER 3 (2021)
(Print) ISSN 1311-0454
(Electronic) ISSN 1314-2224

RESEARCH PAPER

$(N+\alpha)$-ORDER LOW-PASS AND HIGH-PASS FILTER TRANSFER FUNCTIONS FOR NON-CASCADE IMPLEMENTATIONS APPROXIMATING BUTTERWORTH RESPONSE

David Kubanek [1], **Jaroslav Koton** [1],
Jan Jerabek [1], **Darius Andriukaitis** [2]

Abstract

The formula of the all-pole low-pass frequency filter transfer function of the fractional order $(N+\alpha)$ designated for implementation by non-cascade multiple-feedback analogue structures is presented. The aim is to determine the coefficients of this transfer function and its possible variants depending on the filter order and the distribution of the fractional-order terms in the transfer function. Optimization algorithm is used to approximate the target Butterworth low-pass magnitude response, whereas the approximation errors are evaluated. The interpolated equations for computing the transfer function coefficients are provided. An example of the transformation of the fractional-order low-pass to the high-pass filter is also presented. The results are verified by simulation of multiple-feedback filter with operational transconductance amplifiers and fractional-order element.

MSC 2020: 26A33; 93B50, 93C99, 93E11

Key Words and Phrases: fractional-order; analogue filter; transfer function; Butterworth response; non-cascade filter synthesis

1. Introduction

Non-integer-order systems, more commonly called fractional-order (FO) systems, attract attention thanks to their additional degrees of freedom in

pp. 689–714 , DOI: 10.1515/fca-2021-0030 DE GRUYTER

their properties, more flexible characteristics and ability to model various physical phenomena more accurately compared to their integer-order (IO) counterparts [3], [24], [25]. Also analogue frequency filters can be designed as FO. This approach provides more general properties, the most notable of which is the possibility of continuously adjusting the roll-off of the magnitude frequency response without limitation to multiples of 20 dB/dec as is the case of IO filters [6]. FO low-pass (LP) and high-pass (HP) filters feature the stopband slopes of $-20(N+\alpha)$ dB/dec and $+20(N+\alpha)$ dB/dec, respectively, where $N \in \mathbb{N}_0$ is integer component and $\alpha \in (0,1)$ is fractional component of the order, whereas the sum $(N+\alpha)$ is the fractional order of the filter. For example, a 2.4-order LP filter thus provides magnitude frequency response stopband slope of –48 dB/dec. This fine setting of attenuation values in the magnitude response is easily realizable using FO filters over their IO counterparts. The flexible and precise shaping of FO filter characteristics is an efficient feature which finds applications e.g. in biomedical engineering for processing of biological signals such as electrocardiograms (ECG) and electroencephalographs (EEG) [26], for biomedical measurements [9], in microbiological sensor applications [1], control and regulation systems such as FO proportional-integral-derivative (FO PID) controllers [25], [2], or audio signal processing [11].

The design procedures of IO analogue filters are well known, however obtaining a suitable mathematical description (mostly as transfer function (TF) in s-domain, where s is Laplace variable) and circuit implementation of a FO filter is a more complex task. For this purpose, the following two approaches are mainly used:

(1) Numerical search for coefficients of FO TF to minimize the error between the magnitude frequency response of this TF and the selected target function that determines the FO filter requirements over a defined frequency band. In the previous works e.g. the LP Butterworth [6], Chebyshev [5], inverse Chebyshev [7], elliptic [8], arbitrary quality factor [13], flat band-pass [14], and HP Butterworth [17] target magnitude responses have been approximated by the FO filter TF. Once the resulting coefficients of the FO TF are found, it is then usually realized using a circuit derived from a known IO analogue filter, where a classic capacitor is replaced with an element with FO immittance, also known as fractional-order element (FOE), constant phase element (CPE) or simply fractor [23]. The admittance of FOE can be written as $Y(s) = s^{\alpha}F$, where α is a fractional order of FOE, and F is a parameter characterizing FOE referred to as fractance. As the implementations of FOE (mainly

with $\alpha \in (0,1)$, i.e. with capacitive character) are currently being researched intensively and a solid-state FOE is expected to be available soon, it is important to focus on this design approach and to investigate the utilization of FOE in traditional filter topologies to transform these into fractional order. This will reveal potential advantages over their IO counterparts that designers can take advantage of in the future. Currently, due to the commercial unavailability of FOEs, these elements are within experimental verifications often emulated by passive ladder networks consisting of resistors and classic capacitors [27].

(2) The second approach approximates the characteristic of FO filter by a higher IO TF, which is then implemented by an IO circuit of increased complexity but using classic off-the-shelf elements. The early works, e.g. [4], [20], [10], are based on IO approximation of s^α in the FO TF resulting from the first approach, thus in fact two consecutive approximations are carried out. In latter works [16], [18], [19] the IO TF is found directly to approximate the target characteristic of FO filter. However, the drawbacks here are the limited frequency bandwidth and higher number of components (both active and passive) compared to the first approach.

The limitation of the previous works dealing with both approaches is that they are aimed at the design of FO filters of the order between one and two only, i.e. considering $(1+\alpha) \in (1,2)$. Partial attention is paid to higher FO TFs in [6], [4], [20], where the product of a TF with fractional order $(1+\alpha) \in (1,2)$ and a TF with the order $(N-1) \in \mathbb{N}$ is considered to realize $(N+\alpha)$-order FO filter by cascade approach. The problem is that both partial TFs are chosen as Butterworth and thus the resulting filter is no longer Butterworth with maximally flat magnitude response in the passband. In a correct cascade synthesis of Butterworth filters the partial blocks differ in their quality factors. In addition, when the partial filters have the same –3 dB cut-off frequency, their cascade shows a decrease of 6 dB at this frequency. Thus the intended –3 dB cut-off frequency is no longer valid. Assuming the second approach, the resulting IO filter circuits approximating the $(N+\alpha)$-order are more complex, as their order is usually $(N+2)$ and transfer zeros must also be realized. These circuits are more sensitive to the tolerances of element parameters, as we confirm in Section 5.1. The implementation of the FO filters of the order $(N+\alpha)$ using the $(1+\alpha)$-order filter obtained by the first approach and $(N-1)$-order filter, as mentioned in [6], could provide simpler circuits compared to the second approach thanks to utilization of FOE which eliminates the transfer zeros. But the cascade implementation is here probably the only feasible circuit

solution, as the direct realization of the product of the TFs of order $(1+\alpha)$ and $(N-1)$ by a non-cascade structure would be very complicated.

Therefore, in this work the TFs of analogue filters with Butterworth maximally flat magnitude frequency response and fractional order $(N+\alpha)$ higher than two, i.e. with $N \geq 2$, are explored and evaluated for the first time. To better understand the origin of the higher-order FO TF format as defined in Section 2, here we shortly deal with the usual description of $(1+\alpha)$ FO TF. As described e.g. in [6], the second-order LP filter circuits can be transformed to the fractional domain by replacing classic IO capacitor by FOE resulting in one of the following basic forms of FO LP TFs:

$$ {}_1H_{1+\alpha}(s) = \frac{a_0}{b_0 + b_1 s^{\alpha} + b_2 s^{1+\alpha}} , \tag{1.1} $$

$$ {}_2H_{1+\alpha}(s) = \frac{a_0}{b_0 + b_1 s + b_2 s^{1+\alpha}} . \tag{1.2} $$

The order of both these TFs is $(1+\alpha) \in (1,2)$ assuming $\alpha \in (0,1)$ and the coefficients a_0, b_0, b_1, b_2 determine the magnitude and phase frequency response of the filter and can be used to compute the element parameters of the filter circuit. The TFs (1.1) and (1.2) differ in the exponent of s of the denominator term with the b_1 coefficient depending on which of the capacitors in the second-order filter structure is replaced by FOE. The coefficients in (1.1) and (1.2) have been numerically found in [6] to approximate the target Butterworth magnitude response with –3 dB cut-off frequency equal to 1 rad/s and the differences between (1.1) and (1.2) have been analyzed to find out which one is most suitable for approximating the target response. Note that the coefficients a_0, b_0, b_1, b_2 resulting from the numerical search are different for each of the TFs (1.1) and (1.2).

In this article we extend the theory of FO analogue frequency filter TFs and their variant solutions and provide performance and accuracy analysis. The main contribution is the mathematical description and analysis of fractional higher-order TF designated for non-cascade circuit implementations, namely inverse follow-the-leader feedback (IFLF) structure [21] containing only one FOE. For each $(N+\alpha)$-order, all possible variants of all-pole FO LP TF are examined to quantify the differences between them and to determine the most suitable $(N+\alpha)$-order TFs for the approximated Butterworth magnitude responses. The coefficients of these selected TFs are numerically found and expressed in the form of interpolated matrix equations to enable the reader of this article to design the FO filter of up to the $(5+\alpha)$-order. Utilization of the results of these procedures for non-cascade FO HP Butterworth filter design is also briefly mentioned.

2. $(N+\alpha)$-Order Filter Transfer Functions

To introduce the $(N+\alpha)$-order filter TF format, let us start from the $(N+1)$-order IFLF filter structure presented in Figure 2.1, [21].

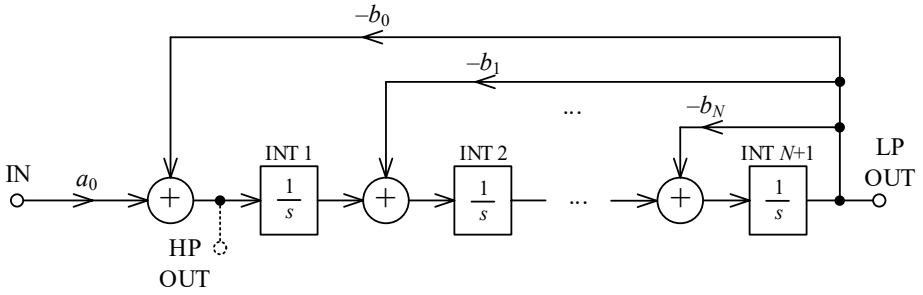

Fig. 2.1: Inverse follow-the-leader feedback (IFLF) structure implementing (2.1).

Its all-pole rational LP TF between the input IN and the output LP OUT is given by

$$H_{N+1}(s) = \frac{a_0}{\sum\limits_{i=0}^{N+1} b_i s^i}\,, \tag{2.1}$$

whereas $b_{N+1} = 1$. Note that the filter order was intentionally chosen $(N+1)$ here for a more convenient notation of the order after extending (2.1) to the fractional domain.

If the k-th IO integrator in the structure in Figure 2.1 is replaced with a fractional one (i.e. with its TF being $1/s^\alpha$) and the other integrators remain unchanged, the TF of the IFLF filter modifies to the FO form

$${}_kH_{N+\alpha}(s) = \frac{a_0}{\sum\limits_{i=0}^{k-1} b_i s^i + \sum\limits_{i=k}^{N+1} b_i s^{i-1+\alpha}} \tag{2.2}$$

with the order $(N+\alpha)$. The comparison of (2.1) and (2.2) reveals that the first k terms in denominator, i.e. with $i \in [0\,..\,(k-1)]$, were not altered and remain with integer exponent of the Laplace variable s. On the other hand, the terms with higher indexes i, i.e. $i \in [k\,..\,(N+1)]$, now contain s raised to the fractional power of $(i-1+\alpha)$. The number of fractional terms in (2.2) is thus $(N+2-k)$. Since the value of k indicates the number of the integrator converted to fractional order in Figure 2.1, its possible range is from 1 to $(N+1)$. The parameter k represents another degree of freedom and extends the variety of TF formats for each filter order $(N+\alpha)$. The suitable choice of k thus must be examined in terms of implementation of the required target frequency response. The described transformation of the filter to fractional domain is advantageous, as only one FOE is required

for the circuit implementation. Note that the IFLF topology is chosen here as an example, but also other multiple-feedback state-variable structures can provide the TF (2.2).

2.1. $(N + \alpha)$-Order Butterworth Low-Pass Transfer Functions.

In this section the coefficients a_0, b_0, b_1, ..., b_N (remember that $b_{N+1} = 1$) of the general $(N + \alpha)$-order TF (2.2) are found using a numerical optimization algorithm to match the target Butterworth LP magnitude response. For each value of the selected filter order $(N+\alpha)$ and possible value of k, an individual search run is carried out resulting in an unique vector of the coefficients $\begin{bmatrix} a_0 & b_0 & b_1 & \dots & b_N \end{bmatrix}$. An optimal k value is found for each considered filter order (combination of N and α) providing the lowest approximation error between the magnitude of (2.2) with the found coefficients and the target function. This optimal value of k then determines that the k-th IO integrator in the filter structure should be replaced by FO integrator and specifies which of the terms in denominator of the TF (2.2) contain s with integer or fractional exponent. Correspondingly, the process can be applied to other approximation types (such as Bessel, Chebyshev, etc.) as well.

The relation for the magnitude of the Butterworth LP transfer function generalized to the fractional order $(N + \alpha)$ that represents the target response in this study is as follows [16], [19]:

$$|B_{N+\alpha}(\omega)| = \frac{1}{\sqrt{1 + \omega^{2(N+\alpha)}}}, \tag{2.3}$$

where ω is angular frequency. This function provides magnitude of –3 dB at cut-off angular frequency 1 rad/s, unity pass-band gain, and stop-band roll-off $-20(N + \alpha)$ dB/dec typical for FO LP filters. Although phase response can also be important for the filter design, we should note that the Butterworth approximation primarily takes into account only the magnitude response which should be maximally flat in the passband. Therefore, we have generalized the known relation valid for integer-order Butterworth filter by utilizing the fractional order $(N + \alpha)$ to obtain the target magnitude response (2.3). Considering the fractional order $(1 + \alpha)$, the relation (2.3) has been also used in previous works dealing with search for FO LP filter TFs with Butterworth response, e.g. in [16], [19]. According to the best authors' knowledge, the mathematical relation, which could be used as a target Butterworth phase response depending on the filter order, does not exist. The phase response can therefore be determined only after the coefficients of the FO TF have been found using the target magnitude response. However, based on the equation (2.2) (considering $s = j\omega$), it is possible to determine the expected asymptotic phase values for very low

and very high frequencies compared to the cut-off frequency 1 rad/s without knowledge of the TF coefficients. The phase response approaches the values 0 and $-90(N+\alpha)$ degrees for low and high frequency respectively.

We have employed numerical optimization to find the coefficients of TF (2.2) such that the maximum absolute error between magnitude in dB of (2.2) and (2.3) is minimized. For this purpose the MATLAB function *fminsearch* was applied with the argument E defined as

$$E = \max_i \left| 20\log|_k H_{N+\alpha}(\boldsymbol{x},\omega_i)| - 20\log|B_{N+\alpha}(\omega_i)| \right|. \tag{2.4}$$

Here $\boldsymbol{x} = \begin{bmatrix} a_0 & b_0 & b_1 & \dots & b_N \end{bmatrix}$ is the sought vector of the coefficients. Each search used $M = 100$ frequency points ω_i logarithmically spaced in the wide frequency range from $\omega_1 = 0.01$ rad/s to $\omega_M = 100$ rad/s, covering both pass-band and stop-band of (2.3). For given N and k, the individual runs of *fminsearch* function were performed for the fractional component α decreasing from $\alpha_{\mathrm{MAX}} = 0.99$ to $\alpha_{\mathrm{MIN}} = 0.01$ with a linear step of $\alpha_{\mathrm{STEP}} = 0.01$. The first search was always performed with the highest $\alpha = 0.99$ because in this case the non-integer exponents of s in (2.2) are as close as possible to the integer exponents in (2.1) and the initial estimation of the sought coefficients (input of *fminsearch* function) can be done on the basis of the well-known coefficients of the Butterworth TF of the integer order $(N+1)$. The next optimization run (with one step lower α) always uses the values of the coefficients determined in the previous run as initial estimation. The pseudocode of the proposed technique of FO TF coefficient design is presented in Algorithm 1. Note that also other minimization criteria (such as mean square error) and search algorithms (e.g. metaheuristic algorithms) can be used, however their investigation is beyond the scope of this paper.

Algorithm 1: Pseudocode of the proposed FO TF coefficient design.

Input: N, k, α_{MAX}, α_{MIN}, α_{STEP}, M, ω_1, ω_M
Output: $\boldsymbol{x_\alpha}$, E_α `// coefficient vector` $\boldsymbol{x}$ `and error` E `for a specific` α
$\boldsymbol{x_0} \leftarrow$ coefficients of $(N+1)$-order Butterworth filter
$\alpha \leftarrow \alpha_{\mathrm{MAX}}$
while $\alpha \geq \alpha_{MIN}$ **do**
  minimize the error E (2.4) with initial point $\boldsymbol{x_0}$
  store $\boldsymbol{x_\alpha}$, E_α
  $\boldsymbol{x_0} \leftarrow \boldsymbol{x_\alpha}$
  $\alpha \leftarrow \alpha - \alpha_{\mathrm{STEP}}$
end
display E_α vs. α

2.2. **Optimization Results.**

The first minimization of E (2.4) was carried out for $N = 2$, thus for fractional order $(N + \alpha) \in (2, 3)$. All the possible k values (i.e. 1, 2, 3) are considered. To evaluate the performance of this optimization it is appropriate to use again the maximum absolute error E in dB defined by (2.4). The resulting values of this error depending on α and k are shown in Figure 2.2.

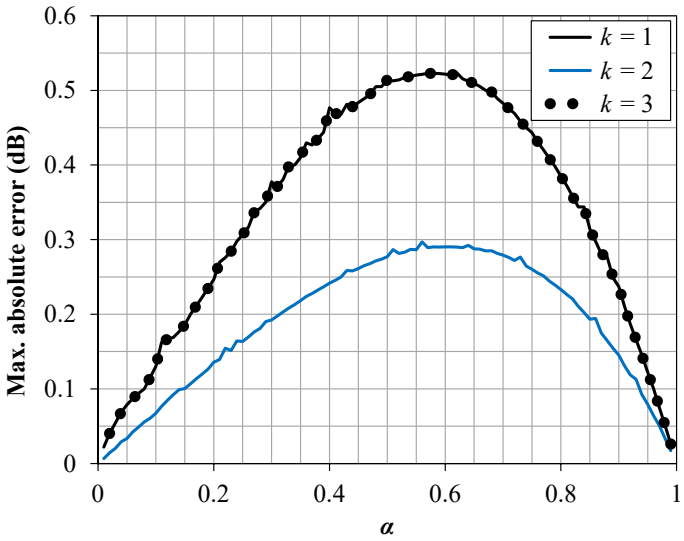

Fig. 2.2: Maximum absolute error between magnitude in dB of (2.2) and (2.3) for $N = 2$.

It is apparent that the magnitude of (2.2) approximates the value of the target function (2.3) with the lowest error for $k = 2$ and values of α close to zero and one. The best results reached for the boundary values of α could be expected, as here TF (2.2) tends to integer order. The maximum error occurs for α around 0.6. Interestingly, the errors for $k = 1$ and $k = 3$ are identical. The value $k = 1$ signifies only one IO term in TF (2.2) and the first integrator of fractional order in Figure 2.1, whereas $k = 3$ denotes only one FO term in (2.2) and the last integrator of fractional order in Figure 2.1. It was also observed that the found values (b_0/a_0), (b_1/a_0), (b_2/a_0), and (b_3/a_0), i.e. the coefficients of the denominator of (2.2) divided by a_0, are identical for both $k = 1$ and $k = 3$. From this point of view it is possible to notice a certain symmetry of the results regarding the value of k.

Similarly, the optimizations were performed for $N = 3$, $N = 4$, and $N = 5$, i.e. for filter orders $(N + \alpha) \in (3, 4)$, $(N + \alpha) \in (4, 5)$, and

$(N+\alpha) \in (5,6)$, respectively, and always with assuming all possible values of k, i.e. $k \in [1\,..\,(N{+}1)]$. The reached maximum absolute errors computed by (2.4) are depicted in Figures 2.3 to 2.5.

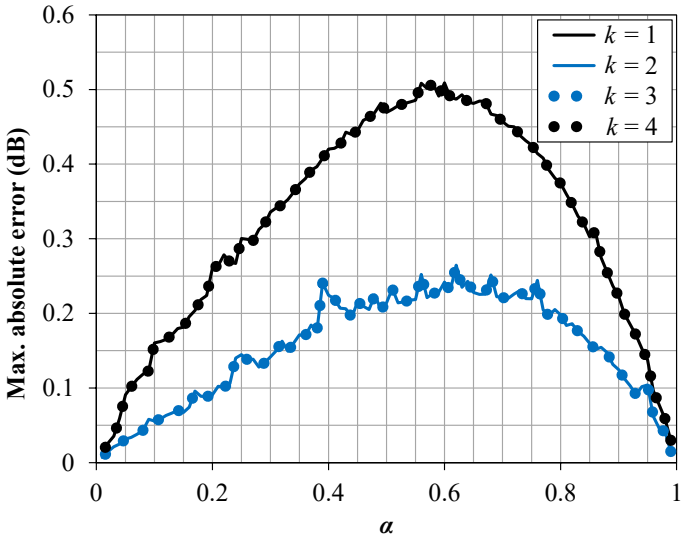

Fig. 2.3: Maximum absolute error between magnitude in dB of (2.2) and (2.3) for $N = 3$.

Also for N values from 3 to 5, the largest approximation errors occur for the boundary (highest and lowest considered) k values. The error is lowest for central values of k, i.e. $k = 2$ and $k = 3$ for $N = 3$, and $k = 3$ for $N = 4$. Up to $N = 4$ the error values show the symmetry with respect to the selected value of k observed already for the case $N = 2$. From the last Figure 2.5 with $N = 5$ it is seen that it is no more possible to unambiguously determine for which value of k from 2 to 5 the error of approximation reaches the smallest value, as the dependences on α are similar for all error curves. Regardless of N, the boundary values of α provide lower error, whereas the highest error is obtained slightly above the middle of the range of α. The achieved absolute error values are almost always below 0.5 dB and for selected optimal values of k they stay below 0.3 dB in the whole range of α, which is a reasonable value. It can be summarized that for $N \in [2\,..\,5]$ and most values of α considered, to reach the best approximation of the target Butterworth response it is recommended to choose k value as follows:

$$k = \begin{cases} N/2+1, & \text{when } N \text{ is even,} \\ (N+1)/2 \text{ or } (N+3)/2, & \text{when } N \text{ is odd.} \end{cases} \tag{2.5}$$

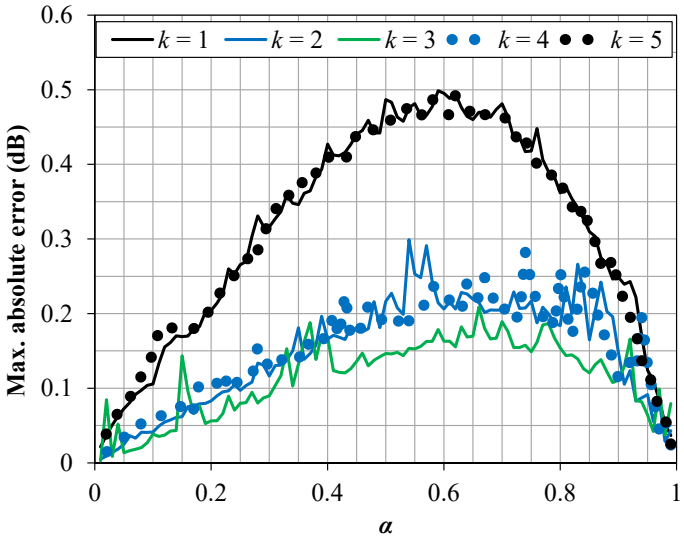

Fig. 2.4: Maximum absolute error between magnitude in dB of (2.2) and (2.3) for $N = 4$.

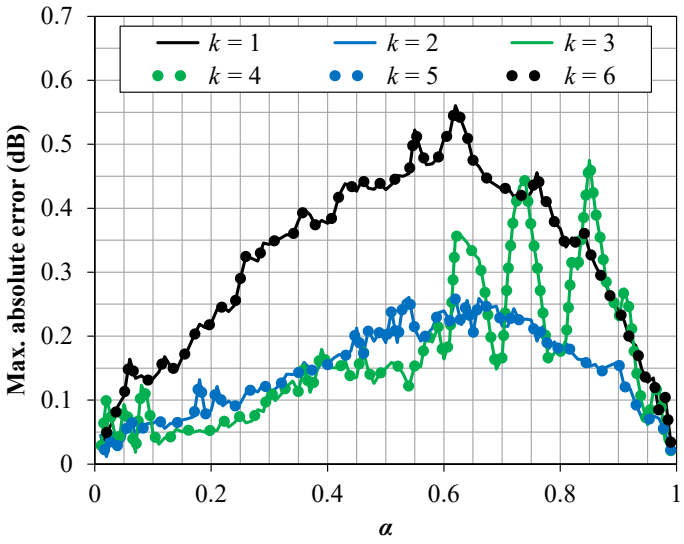

Fig. 2.5: Maximum absolute error between magnitude in dB of (2.2) and (2.3) for $N = 5$.

This optimization, therefore, helps to find the optimal distribution of IO and FO terms in TF (2.2) and also location of FO integrator in the implementing structure, e.g. in Figure 2.1.

The coefficients of the TF (2.2) resulted from the numerical optimization with $N = 2$ and $k = 2$ depending on α are graphically presented by solid lines in Figure 2.6. The coefficients b_1 and b_2 are almost identical, thus their curves (green and violet) overlap. For $\alpha = 0.99$ the values are close to the coefficients of the third-order Butterworth TF which, as already mentioned, have been used as initial estimation for the *fminsearch* function. When decreasing α, the coefficients change continuously and for $\alpha = 0.01$ they approach the coefficients of the second-order Butterworth TF providing that the sum of b_1 and b_2 corresponds to the coefficient of the first power of s in denominator, i.e. 1.414.

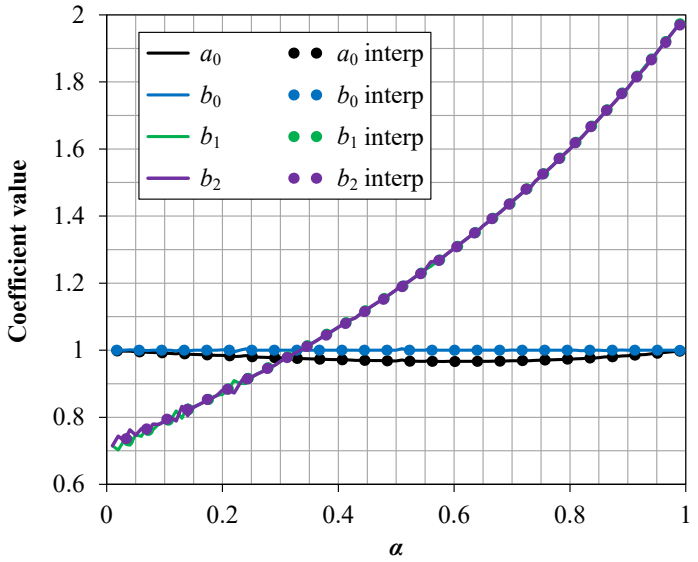

Fig. 2.6: Coefficients of TF (2.2) with $N = 2$ and $k = 2$ found by *fminsearch* function (solid lines) and interpolated by (2.6) (dotted lines).

The following interpolated equations as functions of α have been derived for computing the coefficients a_0, b_0, b_1, ..., b_N. As an example, only one value of k providing the best approximation result is selected for each of the values $N \in [2\,..\,5]$. The coefficient values determined by (2.6) are also displayed in Figure 2.6 by dotted lines to demonstrate the accuracy of the interpolation.

- $\boldsymbol{N = 2}$, $\boldsymbol{k = 2}$

$$\begin{bmatrix} a_0 \\ b_0 \\ b_1 \\ b_2 \end{bmatrix} = \begin{bmatrix} 0.9992 & -0.0720 & -0.0347 & 0.1063 \\ 0.9999 & 0.0005 & 0.0010 & -0.0017 \\ 0.6967 & 0.8991 & -0.1453 & 0.5452 \\ 0.7091 & 0.8101 & 0.0337 & 0.4388 \end{bmatrix} \cdot \begin{bmatrix} 1 \\ \alpha \\ \alpha^2 \\ \alpha^3 \end{bmatrix}. \tag{2.6}$$

- $\boldsymbol{N = 3}$, $\boldsymbol{k = 2}$

$$\begin{bmatrix} a_0 \\ b_0 \\ b_1 \\ b_2 \\ b_3 \end{bmatrix} = \begin{bmatrix} 0.9974 & 0.0421 & 0.0623 & -0.1003 \\ 0.9984 & 0.0973 & 0.1077 & -0.2003 \\ 1.0418 & 1.7942 & -1.0600 & 0.8673 \\ 0.9625 & 0.5066 & 2.8741 & -0.9453 \\ 1.9850 & 1.2112 & 0.0066 & -0.5818 \end{bmatrix} \cdot \begin{bmatrix} 1 \\ \alpha \\ \alpha^2 \\ \alpha^3 \end{bmatrix}. \tag{2.7}$$

- $\boldsymbol{N = 4}$, $\boldsymbol{k = 3}$

$$\begin{bmatrix} a_0 \\ b_0 \\ b_1 \\ b_2 \\ b_3 \\ b_4 \end{bmatrix} = \begin{bmatrix} 0.9958 & 0.0536 & -0.0019 & -0.0487 \\ 0.9917 & 0.1046 & -0.2383 & 0.1461 \\ 2.6217 & 0.9962 & 0.4211 & -0.7971 \\ 1.5721 & 3.1363 & -0.7767 & 1.3395 \\ 1.8296 & 1.1265 & 3.0882 & -0.8161 \\ 2.5946 & 1.2991 & -0.2245 & -0.4183 \end{bmatrix} \cdot \begin{bmatrix} 1 \\ \alpha \\ \alpha^2 \\ \alpha^3 \end{bmatrix}. \tag{2.8}$$

- $\boldsymbol{N = 5}$, $\boldsymbol{k = 2}$

$$\begin{bmatrix} a_0 \\ b_0 \\ b_1 \\ b_2 \\ b_3 \\ b_4 \\ b_5 \end{bmatrix} = \begin{bmatrix} 0.9932 & 0.0931 & -0.1625 & 0.0726 \\ 0.9982 & 0.1058 & -0.0286 & -0.0792 \\ 1.6469 & 3.6925 & -4.2764 & 2.8262 \\ 1.5940 & 0.2503 & 7.0473 & -1.5161 \\ 5.1582 & 5.7095 & -0.7549 & -1.0162 \\ 5.2433 & 1.5986 & -0.0957 & 0.6862 \\ 3.2145 & 1.1127 & -0.1779 & -0.3084 \end{bmatrix} \cdot \begin{bmatrix} 1 \\ \alpha \\ \alpha^2 \\ \alpha^3 \end{bmatrix}. \tag{2.9}$$

3. Stability Verification

It is very important to verify the stability of the TF (2.2) with the coefficients determined by (2.6)-(2.9). The stability was examined using the procedure described in [22] based on converting the s-domain TF to the W-plane. After this transformation the W-domain function is analyzed by classic IO methods. The following steps describe the stability examination:

(1) The substitution $s = W^m$ and $\alpha = n/m$ is performed in FO TF.
(2) The positive integer numbers n and m are chosen such that $\alpha = n/m$.
(3) The poles of the transformed TF, i.e. the roots of the characteristic equation in W-plane, which is of integer order, are found. If

all absolute values of the root angles are higher than $\pi/(2m)$, the system is stable. Otherwise, it is unstable.

Applying this process to the denominator of (2.2) and considering $N = 2$ and $k = 2$ yields the transformed characteristic equation in the W-plane given by

$$b_0 + b_1 W^m + b_2 W^{m+n} + b_3 W^{2m+n} = 0\,. \tag{3.1}$$

For the other selected combinations of N and k providing the best approximation results, the following W-plane characteristic equations are derived from TF (2.2):

- $\boldsymbol{N = 3}$, $\boldsymbol{k = 2}$

$$b_0 + b_1 W^m + b_2 W^{m+n} + b_3 W^{2m+n} + b_4 W^{3m+n} = 0\,. \tag{3.2}$$

- $\boldsymbol{N = 4}$, $\boldsymbol{k = 3}$

$$b_0 + b_1 W^m + b_2 W^{2m} + b_3 W^{2m+n} + b_4 W^{3m+n} + b_5 W^{4m+n} = 0\,. \tag{3.3}$$

- $\boldsymbol{N = 5}$, $\boldsymbol{k = 2}$

$$b_0 + b_1 W^m + b_2 W^{m+n} + b_3 W^{2m+n} + b_4 W^{3m+n} + b_5 W^{4m+n} + b_6 W^{5m+n} = 0\,. \tag{3.4}$$

To analyze the range of α from 0.01 to 0.99 in steps of 0.01 a fixed value of $m = 100$ is chosen which results in integer values of n necessary to satisfy all values of α from the selected range. The minimum absolute values of angles of roots of (3.1)-(3.4) for $0.01 \le \alpha \le 0.99$ and the coefficients determined by (2.6)-(2.9) are presented in Figure 3.1. For reference, the stability margin angle ($180^\circ/(2m) = 180^\circ/200 = 0.9^\circ$) is given as a solid red line. All minimum absolute root angles below this line would indicate unstable behavior.

As it is clear from Figure 3.1, each case has absolute pole angles higher than the stability margin angle. Thus, the filters described by the TF (2.2) with the coefficients given by (2.6)-(2.9) and the respective values of N and k are found to be always stable.

4. **Extension to High-Pass Filters**

Applying the transformation $s \to 1/s$, the FO LP TF (2.2) can be transformed to FO HP TF given by the relation

$${}_kH^{\mathrm{HP}}_{N+\alpha}(s) = \frac{a_0 s^{N+\alpha}}{\sum\limits_{i=0}^{k-1} b_i s^{N+\alpha-i} + \sum\limits_{i=k}^{N+1} b_i s^{N+1-i}}\,. \tag{4.1}$$

Compared to the TF (2.2), there are k fractional terms in the denominator of (4.1) and the term in the numerator is also fractional. The order of the coefficients b in the denominator is reversed (b_0 is in the term with highest

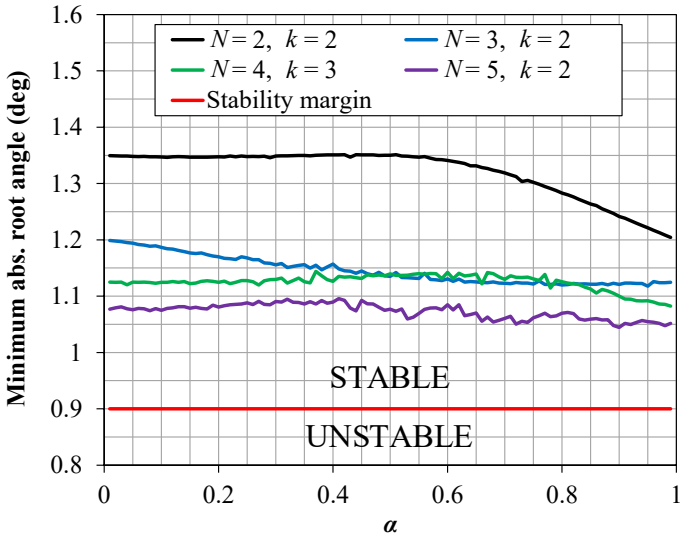

Fig. 3.1: Minimum absolute root angles in W-plane for (3.1)-(3.4).

exponent of s). This HP transfer function can be realized by the IFLF structure in Figure 2.1 with the output marked HP OUT and where the $(N+2-k)$-th integrator is fractional. The coefficients a and b determined for LP TF (2.2) can be used also in HP TF (4.1) to approximate FO HP Butterworth response with –3 dB cut-off frequency 1 rad/s. Therefore no extra numerical search for HP coefficients is required. It is also not necessary to determine for which value of k the lowest deviation of the TF (4.1) from the FO HP Butterworth response is achieved as the optimal value of k is the same as for LP FO TF.

5. Example of the Filter Design and Simulation

As an example, a LP IFLF filter design with order 2.25 and parameters $N = 2$, $k = 2$, $\alpha = 0.25$ will be given. The coefficients of TF (2.2) were found for cut-off angular frequency 1 rad/s. This frequency will be shifted to a more practical value $\omega_0 = 10$ krad/s, i.e. $f_0 = 1592$ Hz, using the frequency scaling demonstrated by the following relation,

$$
\begin{aligned}
{}_2H_{2.25}(s) &= \frac{a_0}{b_0 + \frac{b_1}{\omega_0}s + \frac{b_2}{\omega_0^{1.25}}s^{1.25} + \frac{1}{\omega_0^{2.25}}s^{2.25}} \\
&= \frac{a_0\omega_0^{2.25}}{b_0\omega_0^{2.25} + b_1\omega_0^{1.25}s + b_2\omega_0 s^{1.25} + s^{2.25}}\,.
\end{aligned}
\tag{5.1}
$$

After substitution of the coefficients determined by (2.6) and the selected ω_0 into (5.1) we get

$$ {}_2H_{2.25}(s) = \frac{9.8032 \cdot 10^8}{1 \cdot 10^9 + 9.1933 \cdot 10^4 s + 9.1926 \cdot 10^3 s^{1.25} + s^{2.25}} \,. \qquad (5.2) $$

This TF is realized by the multiple-feedback filter shown in Figure 5.1 containing three operational transconductance amplifiers (OTA), two resistors, two standard capacitors, and one capacitive FOE (F_2 element) with the order $\alpha = 0.25$. The OTA element is a differential voltage-controlled current source with output current given by the product of transconductance gain g_m and differential input voltage: $i_{OUT} = g_m(v_+ - v_-)$. The LT1228 amplifier [15] was used as OTA in the OrCAD PSpice simulations presented here.

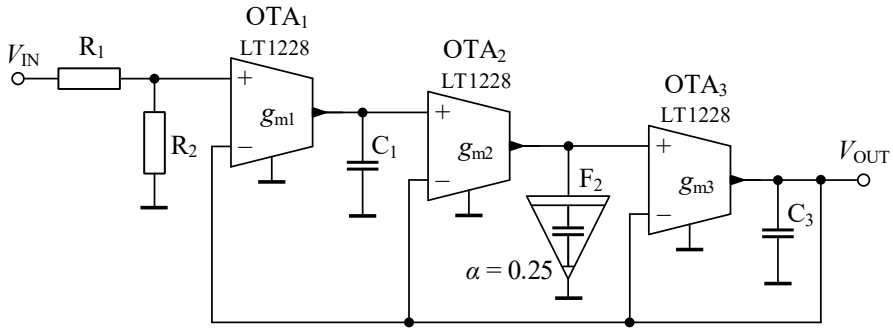

Fig. 5.1: OTA-based 2.25-order LP filter.

The TF of the structure in Figure 5.1 in terms of element parameters is

$$ {}_2H_{2.25}(s) = \frac{\dfrac{R_2}{R_1+R_2}\dfrac{g_{m1}g_{m2}g_{m3}}{C_1F_2C_3}}{\dfrac{g_{m1}g_{m2}g_{m3}}{C_1F_2C_3} + \dfrac{g_{m2}g_{m3}}{F_2C_3}s + \dfrac{g_{m3}}{C_3}s^{1.25} + s^{2.25}} \,. \qquad (5.3) $$

Choosing $C_1 = C_3 = 47$ nF and fractance $F_2 = 63.162$ µF·sec$^{-0.75}$, by comparing the coefficients in denominators of (5.2) and (5.3) we get the transconductances $g_{m1} = 0.5112$ mS, $g_{m2} = 0.6317$ mS, and $g_{m3} = 0.4321$ mS. The DC gain $a_0/b_0 = 0.98032$ is ensured by simple resistive divider $R_1 = 240\ \Omega$, $R_2 = 12$ kΩ at the filter input. Due to the commercial unavailability of FOE, this element was approximated by 7$^{\text{th}}$-order Valsa ladder structure [12] as shown in Figure 5.2. The resistances and capacitances were determined using the approach described in [12] and are summarized

in Table 5.1. The admittance magnitude (black) and phase (blue) characteristics of the approximated FOE (solid lines) and the ideal values (dotted lines) are presented in Figure 5.3. It can be observed that the RC circuit operates correctly in the frequency band from 75 Hz to 1.15 MHz (more than 4 decades) providing the phase angle $90° \cdot \alpha = 22.5°$ with maximum deviation $\pm 1°$.

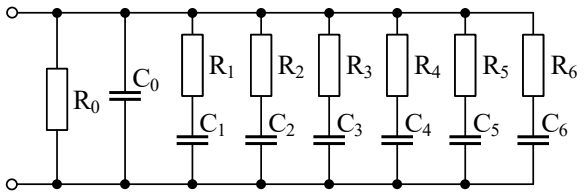

Fig. 5.2: Valsa RC circuit to approximate FOE in Figure 5.1 (F_2 element).

Tab. 5.1: Resistances and capacitances in the circuit from Figure 5.2 ($\alpha = 0.25$, $F_2 = 63.162$ µF $\cdot$ sec$^{-0.75}$).

R_0	4.64 kΩ	C_0	39 pF
R_1	5.11 kΩ	C_1	220 nF
R_2	4.02 kΩ	C_2	33 nF
R_3	6.81 kΩ	C_3	5.6 nF
R_4	1.15 kΩ	C_4	1.2 nF
R_5	2.2 kΩ	C_5	4.7 nF
R_6	590 Ω	C_6	270 pF

The PSpice simulated magnitude frequency characteristic of the filter from Figure 5.1 with LT1228 OTAs and FOE from Figure 5.2 is depicted in Figure 5.4 as dotted black line. The target characteristic determined by (2.3) and shifted to the cut-off frequency $f_0 = 1592$ Hz is represented by black solid line. The optimized magnitude characteristic given by (5.2) is displayed by dashed black line. The blue and green lines have been added to illustrate the position of the FO characteristics between the 2$^{\text{nd}}$ and 3$^{\text{rd}}$ filter order.

Both the optimized and simulated characteristics of the filter are in a very good agreement with the target function. As these characteristics overlap, the magnitude errors of the optimized function and of the simulated

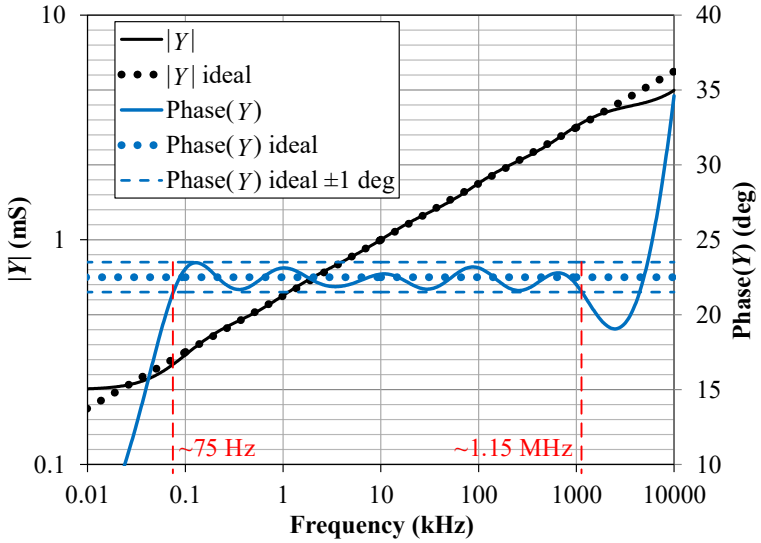

Fig. 5.3: Admittance magnitude and phase characteristics of the approximated FOE from Figure 5.2.

characteristic against the target function are shown in Figure 5.5 by the dashed and dotted lines, respectively.

The error of the optimized characteristic (5.2) with the found coefficients vs. the target function is in the range of ±0.17 dB which confirms also the result in Figure 2.2 (blue line at $\alpha = 0.25$). The error of the simulated characteristic follows the error of the optimized characteristic up to 1 kHz and at higher frequency it turns to negative values, however it does not exceed a very low value of –0.72 dB in the displayed band.

The phase frequency characteristics of the optimized function (5.2) and of the simulated filter from Figure 5.1 are shown in Figure 5.6 by dashed and dotted lines, respectively. Target phase is not present in Figure 5.6 as only magnitude part is defined by the target function (2.3). As discussed in the Section 2.1, a target phase response in a form of mathematical relation cannot be defined. Thus only the asymptotic phase values $0°$ and $-90° \cdot 2.25 = -202.5°$, which the phase theoretically approaches at the edges of the frequency band, are indicated by the red arrows in Figure 5.6. Both of the black phase characteristics in the figure are close to each other and approach the expected asymptotic values at low and high frequencies. The phase characteristics of the 2^{nd} and 3^{rd} order Butterworth filter have been also added for illustration. Both of the black phase characteristics are close to each other and at high frequencies they approach the expected

value $-90° \cdot 2.25 = -202.5°$. Figure 5.7 displays the difference between the simulated phase characteristic and the optimized phase of (5.2) from Figure 5.6 in detail.

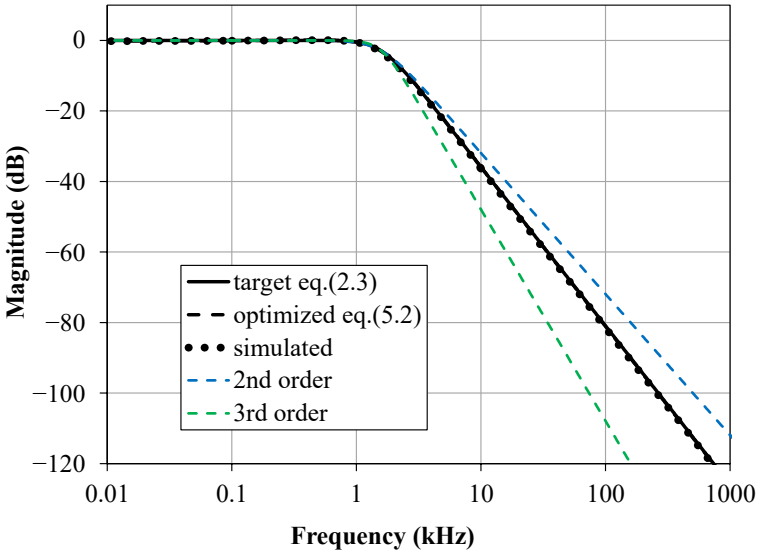

Fig. 5.4: Target acc. to (2.3) (solid black), optimized acc. to (5.2) (dashed black), and simulated (dotted black) magnitude characteristics of the Butterworth LP filter of the order 2.25. (The black lines overlap.)

5.1. **Monte-Carlo Analysis.**

In order to determine the sensitivity properties of the circuit in Figure 5.1, the Monte-Carlo (MC) simulations considering 10 % tolerance values (drawn from a uniform distribution) for the resistors, capacitors, and FOE were performed for 200 runs. The OTAs were simulated with exact transconductance gains, as these parameters can be precisely set for the amplifiers via an external control input. The resulting MC magnitude responses are presented in Figure 5.8 by green lines and the nominal run (with exact element values) is marked with black color. The inset shows a detail of the characteristics around the cut-off frequency 1.592 kHz. It is apparent that the circuit has low sensitivity to the variations of passive element values, especially in the passband. For example at 0.1 kHz the maximum magnitude deviation from the nominal run is 0.04 dB and in the stopband at 10 kHz this deviation is 2.1 dB. The –3 dB cut-off frequency of the runs varies between 1.38 kHz and 1.81 kHz.

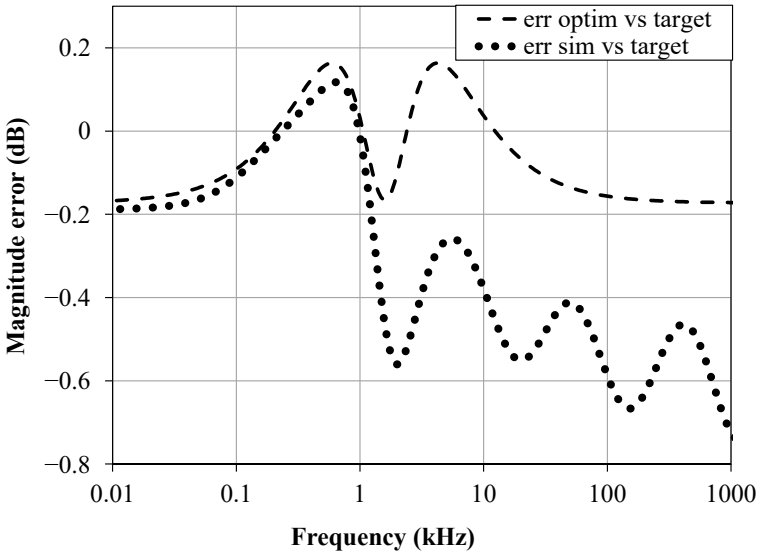

Fig. 5.5: Magnitude errors of optimized (5.2) (dashed), and simulated (dotted) characteristics from Figure 5.4 vs. target function (2.3).

To have a possibility of comparison with other works, the MC simulations were carried out also for a 4.5-order LP Butterworth filter with $N = 4$, $\alpha = 0.5$, $k = 3$, TF according to (2.2), and coefficients calculated by (2.8). The TF was implemented by the non-cascade IFLF structure analogous to Figure 5.1 which was extended by two integrator sections. The MC responses are shown in Figure 5.9. The frequency axis is normalized with regard the cut-off frequency for the sake of generality. The results again confirm that also the 4.5-order filter has low sensitivity, mainly in the passband. At the normalized frequency 0.1 the maximum magnitude deviation from the nominal run is 0.09 dB and in the stopband at frequency 10 this deviation is 2.9 dB. The normalized –3 dB cut-off frequency of the runs is detected between 0.76 and 1.19.

The MC simulations in Figure 5.9 were compared with the following TF presented in [19] as equation (13):

$$H_{4.5}(s) = \frac{0.0241s^2 + 0.6159s + 1.2501}{(0.1696s^3 + 1.3706s^2 + 2.0965s + 1.2433)(s+1)(s^2+s+1)}\,. \tag{5.4}$$

This TF approximates also the 4.5-order Butterworth LP response by a product of three integer-order LP TFs. The 3$^{\text{rd}}$ order TF with transfer

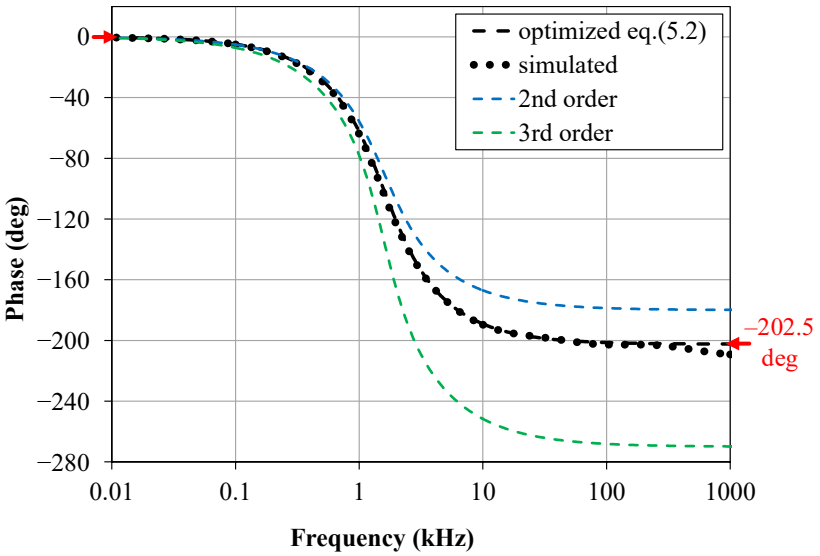

Fig. 5.6: Optimized acc. to (5.2) (dashed), and simulated (dotted) phase characteristics of the Butterworth LP filter of the order 2.25.

zeros approximates the 1.5-order Butterworth response. The 1st and 2nd order all-pole TFs, having together a Butterworth response, increase the filter order by three. Each of the mentioned individual parts of the TF (5.4) were implemented using the follow-the-leader feedback (FLF) circuits with current feedback operational amplifiers (CFOA) presented in [19]. Apparently, this structure cascaded of three circuits is much more complex in comparison to the 4.5-order IFLF filter used for the previous simulation. The MC simulations of the structure from [19] are depicted in Figure 5.10. It is evident that this circuit is more sensitive than the 4.5-order filter from this work, especially in the passband. Here at the normalized frequency 0.1 the maximum magnitude deviation from the nominal run is 4.1 dB and in the stopband at frequency 10 this deviation is 5.2 dB. The normalized –3 dB cut-off frequency of the MC runs is between 0.57 and 1.01 and the nominal run shows the cut-off frequency of only 0.81, whereas at the unity frequency the nominal run decreases to –6 dB. It confirms that the 4.5-order filter from [19] does not provide an exact Butterworth response because the partial cascaded TFs are chosen as Butterworth, as discussed in Section 1.

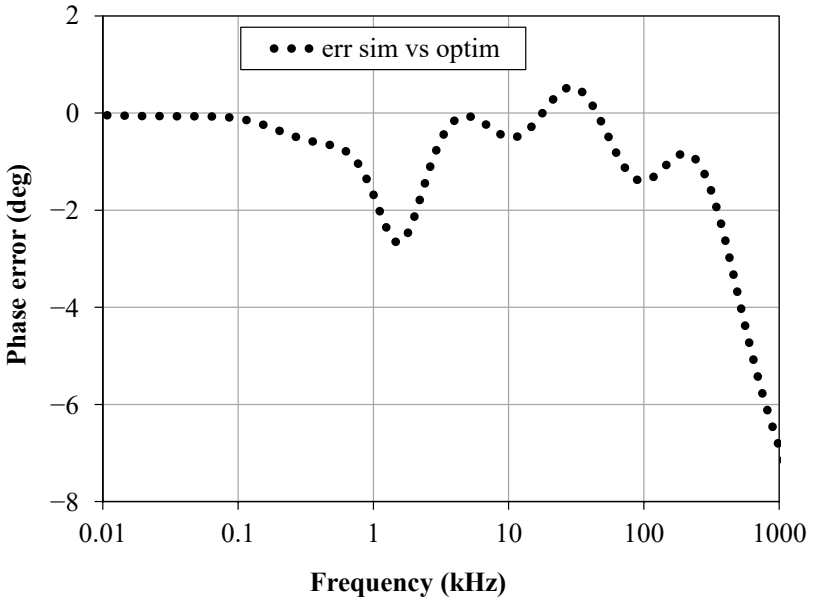

Fig. 5.7: Phase error of simulated and optimized acc. to (5.2) characteristics from Figure 5.6.

6. **Discussion and Conclusion**

We have introduced formats of all-pole LP and HP filter TFs of the fractional order higher than two, suitable for non-cascade circuit implementations, e.g. by state-variable structures with integrators and multiple feedbacks. The LP TFs of the fractional order from 2 to 6 have been examined regarding the accuracy of the approximation of the Butterworth target function. Their slope of magnitude frequency response in stopband is continuously adjustable between –40 dB/dec and –120 dB/dec and not limited to multiples of 20 dB/dec only, which is an important difference compared to IO filters. All the FO TF formats considered (depending on the selected values of N and k) show good agreement with the target function, while the maximum absolute error is mostly below 0.5 dB. The error can be reduced even below 0.3 dB with the optimal choice of the value of k determining the position of the FO integrator in the filter structure. It was found that the FO integrator should be located in the middle of the structure and for higher filter orders it should not at least occur at its edge to reach the lowest error of approximation of the target function. For these most suitable values of k and fractional orders from 2 to 6 the relations for computing the FO TF coefficients are presented.

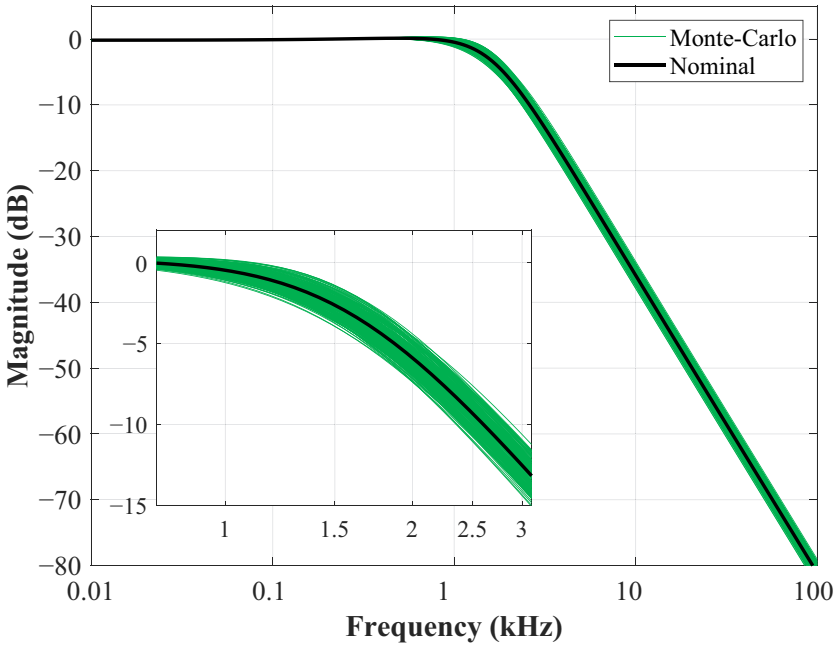

Fig. 5.8: Monte-Carlo simulated magnitude characteristics of the 2.25th-order Butterworth LP filter.

The resulting FO filter structure differs from the conventional IO one only in replacing one standard capacitor with FOE. With the expected availability of FOE implementations, it will be possible to easily design FO filters without increasing the circuit complexity compared to conventional IO filters. The structures with integrators and multiple feedbacks are practically well-proven and employ commonly available active elements.

FO HP filters can be easily obtained from the FO LP filters by the well-known $s \to 1/s$ transformation of the TF. The described methodology can also be used to design FO filters based on other target functions (e.g. Chebyshev, Cauer, Bessel), but for this purpose it is necessary for the designer to program own optimization routine for finding the TF coefficients and possibly use a modified filter structure with feedforwards in case the TF contains transfer zeros.

Acknowledgements

The research results described in this paper are supported by The Czech Science Foundation, Project No. 19-24585S. This article is based upon work from COST Action CA15225, a network supported by COST (European Cooperation in Science and Technology).

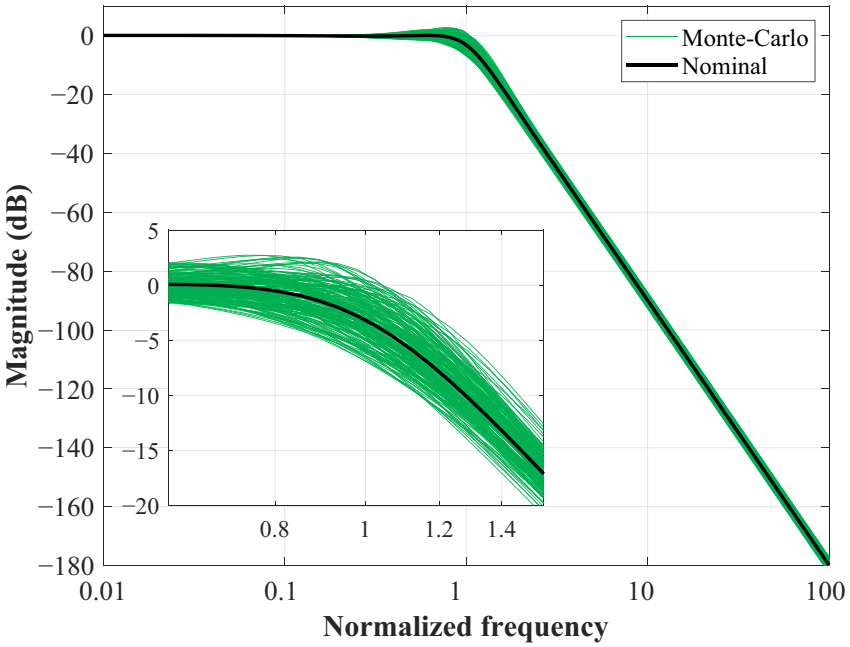

Fig. 5.9: Monte-Carlo simulated magnitude characteristics of the 4.5th-order Butterworth LP filter from this work.

References

[1] K. Biswas, S. Sen, P.K. Dutta, A constant phase element sensor for monitoring microbial growth. *Sens. Actuators B Chem.* **119**, No 1 (2006), 186–191; DOI: 10.1016/j.snb.2005.12.011.

[2] K. Biswas, G. Bohannan, R. Caponetto, A.M. Lopes, J.A.T. Machado, *Fractional-Order Devices*. Springer, Berlin/Heidelberg, Germany (2017); DOI: 10.1007/978-3-319-54460-1.

[3] A.S. Elwakil, Fractional-order circuits and systems: An emerging interdisciplinary research area. *IEEE Circuits Syst. Mag.* **10**, No 4 (2010), 40–50; DOI: 10.1109/MCAS.2010.938637.

[4] T.J. Freeborn, B. Maundy, A.S. Elwakil, Field programmable analogue array implementation of fractional step filters. *IET Circuits Devices and Syst.* **4**, No 6 (2010), 514–524; DOI: 10.1049/iet-cds.2010.0141.

[5] T. Freeborn, B. Maundy, A.S. Elwakil, Approximated fractional order Chebyshev lowpass filters. *Math. Probl. Eng.* **2015** (2015), 1–7; DOI: 10.1155/2015/832468.

[6] T.J. Freeborn, Comparison of $(1+\alpha)$ fractional-order transfer functions to approximate low pass Butterworth magnitude responses. *Circuits,*

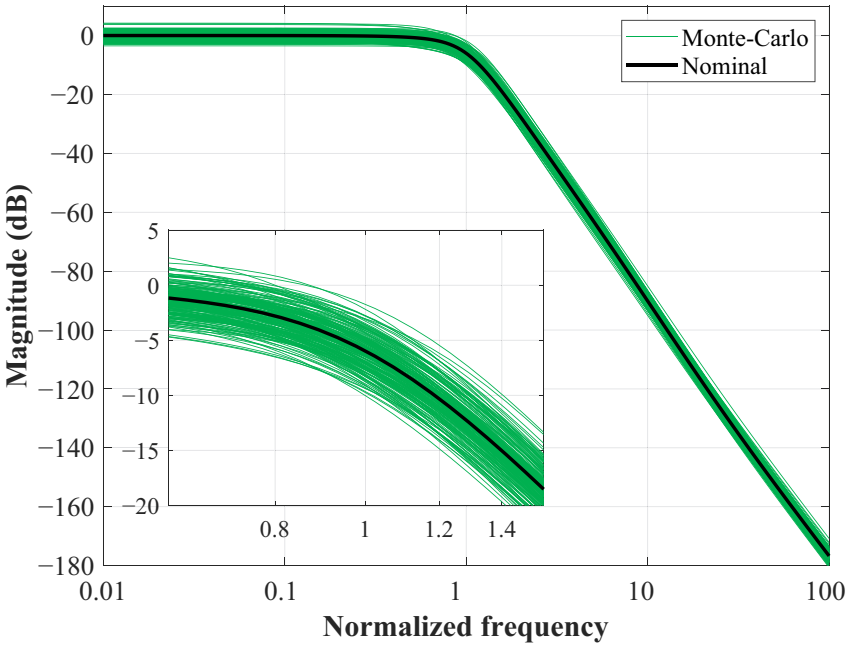

Fig. 5.10: Monte-Carlo simulated magnitude characteristics of the 4.5th-order Butterworth LP filter from [19].

Syst. Signal Process. **35** (2016), 1983–2002; DOI: 10.1007/s00034-015-0226-y.

[7] T.J. Freeborn, A.S. Elwakil, B. Maundy, Approximated fractional-order inverse Chebyshev lowpass filters. *Circuits, Syst. Signal Process.* **35** 2016, 1973–1982; DOI: 10.1007/s00034-015-0222-2.

[8] T.J. Freeborn, D. Kubanek, J. Koton, J. Dvorak, Validation of fractional-order lowpass elliptic responses of $(1 + \alpha)$-order analog filters. *Appl. Sci.* **8**, No 12 (2018), 1–17, DOI: 10.3390/app8122603.

[9] D. Gupta, C.A. Lammersfeld, P.G. Vashi, J. King, S.L. Dahlk, J.F. Grutsch, C.G. Lis, Bioelectrical impedance phase angle as a prognostic indicator in breast cancer. *BMC Cancer* **8**, No 249 (2008), DOI: 10.1186/1471-2407-8-249.

[10] E.M. Hamed, A.M. AbdelAty, L.A. Said, A.G. Radwan, Effect of different approximation techniques on fractional-order KHN filter design. *Circuits, Syst. Signal Process.* **37** (2018), 5222–5252; DOI: 10.1007/s00034-018-0833-5.

[11] T. Helie, Simulation of fractional-order low-pass filters. *IEEE/ACM Trans. Audio, Speech, Language Process.* **22**, No 11 (2014), 1636–1647; DOI: 10.1109/TASLP.2014.2323715.

[12] A. Kartci, A. Agambayev, M. Farhat, N. Herencsar, L. Brancik, H. Bagci, K.N. Salama, Synthesis and optimization of fractional-order elements using a genetic algorithm. *IEEE Access* **7** (2019), 80233–80246; DOI: 10.1109/ACCESS.2019.2923166.

[13] D. Kubanek, T. Freeborn, $(1 + \alpha)$ fractional-order transfer functions to approximate low-pass magnitude responses with arbitrary quality factor. *Int. J. Electron. Commun. (AEU)* **83** (2018), 570–578; DOI: 10.1016/j.aeue.2017.04.031.

[14] D. Kubanek, T. Freeborn, J. Koton, Fractional-order band-pass filter design using fractional-characteristic specimen functions. *Microelectron. J.* **86** (2019), 77–86; DOI: 10.1016/j.mejo.2019.02.020.

[15] Linear Technology. LT1228 100 MHz Current Feedback Amplifier with DC Gain Control. Datasheet, 2012.

[16] S. Mahata, S.K. Saha, R. Kar, D. Mandal, Optimal design of fractional order low pass Butterworth filter with accurate magnitude response. *Digit. Signal Process.* **72**, No C (2018), 96–114; DOI: 10.1016/j.dsp.2017.10.001.

[17] S. Mahata, R. Kar, D. Mandal, Optimal fractional-order highpass Butterworth magnitude characteristics realization using current-mode filter. *Int. J. Electron. Commun. (AEU)* **102** (2019), 78–89; DOI: 10.1016/j.aeue.2019.02.014.

[18] S. Mahata, S. Saha, R. Kar, D. Mandal, Optimal integer-order rational approximation of α and $\alpha + \beta$ fractional-order generalised analogue filters. *IET Signal Process.* **13**, No 5 (2019), 516–27; DOI: 10.1049/iet-spr.2018.5340.

[19] S. Mahata, S. Banerjee, R. Kar, D. Mandal, Revisiting the use of squared magnitude function for the optimal approximation of $(1 + \alpha)$-order Butterworth filter. *Int. J. Electron. Commun. (AEU)* **110** (2019), 1–11; DOI: 10.1016/j.aeue.2019.152826.

[20] B. Maundy, A.S. Elwakil, T.J. Freeborn, On the practical realization of higher-order filters with fractional stepping. *Signal Process.* **91**, No 3 (2011), 484–491; DOI: 10.1016/j.sigpro.2010.06.018.

[21] D.J. Perry, New multiple feedback active RC network. *Electron. Lett.* **11**, No 16 (1975), 364–365; DOI: 10.1049/el:19750278.

[22] A.G. Radwan, A.M. Soliman, A.S. Elwakil, A. Sedeek, On the stability of linear systems with fractional-order elements. *Chaos Solitons Fractals* **40**, No 5 (2009), 2317–28; DOI: 10.1016/j.chaos.2007.10.033.

[23] Z.M. Shah, M.Y. Kathjoo, F.A. Khanday, K. Biswas, C. Psychalinos, A survey of single and multi-component Fractional-Order Elements (FOEs) and their applications. *Microelectron. J.* **84** (2019), 9–25; DOI: 10.1016/j.mejo.2018.12.010.

[24] H.G. Sun, Y. Zhang, D. Baleanu, W. Chen, Y.Q. Chen, A new collection of real world applications of fractional calculus in science and engineering. *Commun. Nonlinear Sci. Numer. Simul.* **64** (2018), 213–31; DOI: 10.1016/j.cnsns.2018.04.01.

[25] A. Tepljakov, *Fractional-order Modeling and Control of Dynamic Systems*. Springer International Publishing, Berlin/Heidelberg, Germany (2017); DOI: 10.1007/978-3-319-52950-9.

[26] G. Tsirimokou, C. Psychalinos, A.S. Elwakil, *Design of CMOS Analog Integrated Fractional-Order Circuits: Applications in Medicine and Biology*. Springer, Berlin/Heidelberg, Germany (2017); DOI: 10.1007/978-3-319-55633-8.

[27] J. Valsa, J. Vlach, RC models of a constant phase element. *Int. J. Circuit Theory Appl.* **41**, No 1 (2013), 59–67; DOI: 10.1002/cta.785.

[1] *Dept. of Telecommunications*
Faculty of Electrical Engineering and Communication
Brno University of Technology
Technicka 3082/12
616 00 Brno, CZECH REPUBLIC

e-mail: kubanek@feec.vutbr.cz (Corresponding author)
Received: January 30, 2021, Revised: March 22, 2021
e-mails: koton@feec.vutbr.cz , jerabekj@feec.vutbr.cz

[2] *Dept. of Electronics Engineering*
Kaunas University of Technology
Studentu St. 50-438
LT-51368 Kaunas, LITHUANIA

ad e-mail: darius.andriukaitis@ktu.lt

Please cite to this paper as published in:

Fract. Calc. Appl. Anal., Vol. **24**, No 3 (2021), pp. 689–714,
DOI: 10.1515/fca-2021-0030